First-principles study on photovoltaic properties of 2D Cs$_2$PbI$_4$-black phosphorus heterojunctions

Yu-Qing Zhao[1,2,6] (ORCID)**, Ying Xu**[1]**, Dai-Feng Zou**[1] (ORCID)**, Jun-Nian Wang**[1]**,
Guo-Feng Xie**[2]**, B Liu**[3]**, Meng-Qiu Cai**[4,6] (ORCID) **and Shao-Long Jiang**[5,6]

[1] School of Physics and Electronics Science, Hunan University of Science and Technology, Xiangtan 411201, Peoples's Republic of China
[2] Hunan Provincial Key Laboratory of Advanced Materials for New Energy Storage and Conversion, Xiangtan 411201, People's Republic of China
[3] Hunan Key Laboratory for Super-Microstructure and Ultrafast Process, School of Physics and Electronics, Central South University, Changsha 410083, Hunan, People's Republic of China
[4] School of Physics and electronics Science, Hunan University, Changsha, Hunan 410082, People's Republic of China
[5] Department of Materials Science and Engineering, College of Engineering, Peking University, Beijing 100871, People's Republic of China

E-mail: yqzhao@hnu.edu.cn (Y Q Zhao), mqcai@hnu.edu.cn (M Q Cai) and jiangsl-cnc@pku.edu.cn (S L Jiang)

Abstract

Both 2D perovskite Cs$_2$PbI$_4$ and phosphorus are significant optoelectronic semiconductor materials, the optical-electrical characters between both contact interfaces are interesting topics. In present work, we demonstrate comparative investigation of optoelectronic properties for two kinds of electrical contact interfaces. i.e. Pb–I and Cs–I interfaces with black phosphorus contacts. The carrier transport, charge transferring and optical properties for both cases are investigated by using first principle calculation. Both contact interfaces exhibit type II band alignment with direct band gap. Charge carrier migration from Cs–I interface to black phosphorus is more strong than that of Pb–I interface by considering differential charge density and bader charge between distinct electrical contact interfaces. Besides, electron–hole effective masses of heterojunctions for both cases along different direction are investigated. Optical absorption coefficients of both cases are compared with those of free-standing Cs$_2$PbI$_4$ and black phosphorus in the visible spectrum. We systematically compared advantages and disadvantages of two kinds of contact interfaces for photovoltaic application, and the results reveal interfacial engineering of 2D heterojunction plays a important role in tuning optoelectronic properties.

Keywords: 2D heterojunction, first-principles, carrier effective masses, charge transfer, optical property, electronic structures

S Supplementary material for this article is available online

(Some figures may appear in colour only in the online journal)

---

[6] Author to whom anys correspondence should be addressed.

1. Introduction

Solar energy is renewable and clean energy, which is essential for the sustainable development of human beings. Searching for new photovoltaic material, which adapts to lower manufacturing cost, higher conversion efficiency and resistance to oxidation and humidity, is crucial and eternal challenges. In the past few year, organic–inorganic hybrid perovskite materials have made significant breakthroughs in the field of photovoltaics due to the superior photovltaic property [1–4], and current certified photoelectric conversion efficiency has exceeded 23.5%.[5] Organic–inorganic hybrid perovskite materials can be divided into three-dimensional (3D) and two-dimensional (2D) crystal structure according to spatial dimensionality. The 3D hybrid perovskite materials have general formula ABX_3, where A is orgainic molecule or inorganic element, B is metallic, and X is halogen element. Among them, the most typical one is lead-based perovskite material $MAPbI_3$, and the geometric construction, electronic structure, optical absorption, electron–phonon coupling as well as charge carrier property has been in-depth investigated theoretically and experimentally as solar absorbers [6–11]. Although high photoelectric conversion efficiency for 3D crystal structure has been achieved, the instability due to corrosion while exposed to air is still a major drawback to restrict their wide usage and commercialization [12]. The newly synthetic 2D perovskite [13] with the formula $A_{n-1}B_nX_{3n+1}$ is believed and confirmed to be more stable than that of 3D perovskite due to layered octahedral structures BX_6^- separated by organic molecular groups or inorganic ions, which can prevent octahedral BX_6^- decomposing effectively. Currently, many theoretical studies about 2D perovskite have been carried out. For instance, Dong *et al* [14] theoretically investigated the effects of mixed cations (Cs + and Rb+) and metal ions (Ge^{2+} and Pb^{2+}) of $(RNH_3)_2(MA)_{n-1}B_nX_{3n+1}(n=3)$ on the solar harvesting to electricity efficiency, demonstrating tuning appropriate composition ratio can improve efficiency and stability. Ding *et al* [15] reported that optical absorption and transport property of single-layer 2D perovskite Cs_2PbI_4 are strongly depend on the layers *n*. Additionally, Bala *et al* [16] calculated electronic structure of multilayered 2D perovskite $Cs_{n+1}Sn_{n-x}I_{3n+1}$, and results reveal that band gaps, thermal stability and optical property of multilayered 2D perovskite vary with layer *n*.

Phosphorene, a single-layered semiconductor material derived from black phosphorus, belongs to the family of two-dimensional (2D) layered materials. Due to the unique physical properties such as superior electronic properties, strong optical transparency and extraordinary charge carrier mobilities, this material is considered to play potential major roles in the field of photovoltaic solar cell [17–19]. Thus, constructing 2D perovskite and phosphorene heterojunction and investigating their interfacial properties is an essential and significant topic. Liu *et al* makes a comparative study of interfacial properties of 2D perovskite BA_2XBr_4 (BA = $(C_4H_9NH_3)_2$, X = Pb, Sn Ge) and phosphorene heterojunction, and they concluded that M_2GeBr_4-BP heterostructure is most suitable for photovoltaic application [20]. However, various interfacial contacts have not been considered in detail. Liu [20]
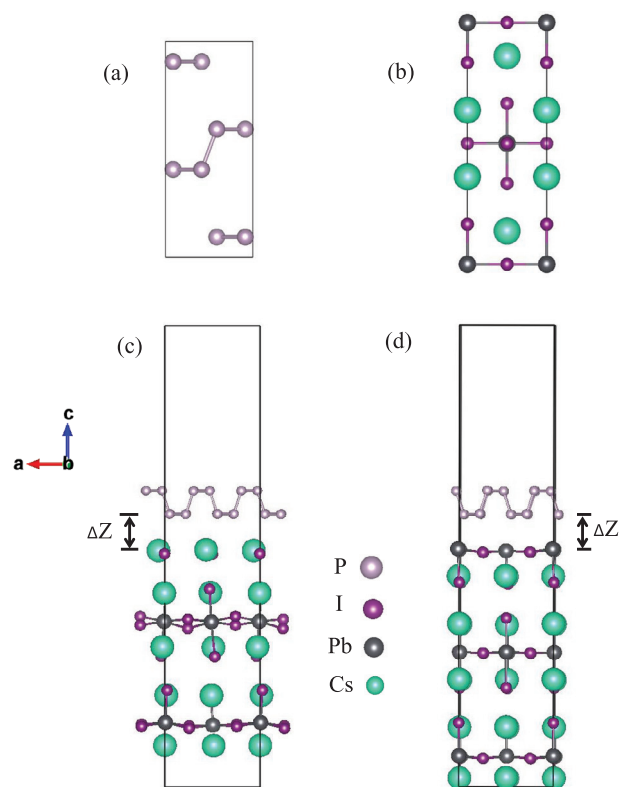
Figure 1. (a) atomic structure of (a) black phosphorous and (b) layered perovskite Cs_2PbI_4 preparing to construct two-dimensional heterojunction. (c) Cs–I interface contact and (d) Pb–I interface contact of heterojunction with black phosphorous. The gray, purple, dark, and cyan balls respect P, I, Pb, Cs atoms, respectively.

and Zhang [21] investigated chemical, mechanical stability and charge transferring property of 3D $APbI_3$(A = CH_3NH_3, Cs)-black phosphorus heterojunction with different terminal, and concluded that mechanical stability and charge transfer of 3D perovskite $APbI_3$-black phosphorus heterojunction are insufficient. Chen *et al* [22] synthesize mixed-dimensional 0D–2D heterostructure $CsPbBr_3$-black phosphorus via an *in situ* technique, verifying fast carrier transfer between $CsPbBr_3$ and phosphorus layers. Yang *et al* [23] theroretically explored the optoelectronic porperty of 3D–2D heterostructure $CsSnI_3$-black phosphorus, demonstrating type I and type II band alignment for I–Cs and I–Sn interface, respectively. However, to our known, there are still lack of theoretical investigation of full two-dimensional 2D–2D perovskite-black phosphorus heterojunctions with different interfacial contacts.

In this work, we firstly construct 2D single layer Cs_2PbI_4 and phosphorene heterojunction with different terminal contacts, i.e. Cs–I and Pb–I interface contacts. Based on the optimized structure, the thermal stability of different interfacial terminals were comparatively calculated and investigated. Besides, electronic structures of the heterojunction with two interfacial contacts were calculated to analyze the heterojunction band alignment type and origin of photogenerated carriers, which can be conductive to comprehensive photovoltaic mechanism of 2D heterostructure. Moreover, charge carrier effective masses, electron charge transferring, optical absorption coefficients of Cs_2PbI_4–P heterojunction with different

Table 1. Calculated lattice parameter (a) and (b); interlayer distances ΔZ between Cs_2Pb_4 and P layers and interface adhesion energies Eb for Cs–I and Pb–I interfacial contacts, respectively.

	ΔZ (Å)	a (Å)	b (Å)	Eb (eVÅ^{-2})
Cs–I interface	3.28	8.75	9.82	−1.37
Pb–I interface	3.20	8.67	9.77	−1.51

interfacial contacts were calculated and investigated qualitatively and quantitatively for comparison to search more superior interface with outstanding photovoltaic performance.

2. Computational methods

All calculations were performed by using the Vienna *ab initio* simulation package (VASP) [24, 25] with the projector augmented-wave (PAW) method [26]. The exchange and correlation potential was described by the Perdew–Burke–Ernzerhof (PBE) of generalized gradient approximation (GGA) functiona [27]. The valence electron configuration for Cs, Pb, I, P were $5s^25p^66s^1$, $6s^26p^2$, $5s^25p^5$, $3s^23p^3$, respectively. Two kinds of electrical interfacial contacts i.e. Cs–I and Pb–I (0 0 1) with monolayer black phoshrous (0 0 1) surface were constructed into 2D heterojunction with 15 Å vacuum thickness, and the weak bonds between different interface were indicated by vdw-D2 method [28] correction to describe Van der Waals force. A kinetic energy cutoff of 400 eV was selected for the plane-wave basis set for all calculations, and a $4 \times 4 \times 1$ Monkhorst–Pack k point meshes were employed to fully optimize geometric structure until the convergence criteria of energy and force on each atom were below 10^{-5} eV and -0.02 eV·Å^{-1}, respectively. Heyd–Scuseria–Ernzerhof hybrid functional (HSE06), which mixes the exchange density functional with a fraction of 25% Fock exchange energy, were adopted to calculate electronic structure to correct the electron interaction [29]. For calculation of optical properties, more dense $6 \times 6 \times 1$ grid of k points were employed. Figures were plotted by using the VESTA and Origin packages.

The electron–hole effective masses along Γ–X and Γ–Y directions in *a-b* plane were calculated, respectively by utilizing the band edge to solve the second derivative according to the following formula:

$$m* = \hbar^2 \left[\frac{\partial^2 \varepsilon(k)}{\partial k^2} \right]^{-1}. \quad (1)$$

Where the $\hbar$ is the planck constant, the $\varepsilon(k)$ represents the band energy eigenvalues, and the k indicates the wave vector along Γ–X and Γ–Y directions.

To calculate optical property calculation, the complex dielectric function $\varepsilon(\omega) = \varepsilon_1(\omega) + i\varepsilon_2(\omega)$, which contains real part $\varepsilon_1(\omega)$ and imaginary part $\varepsilon_2(\omega)$, was evaluated, where $\varepsilon_1(\omega)$ is obtained from $\varepsilon_2(\omega)$ by using the Kramers–Kronig relationship. Absorption coefficients of 2D heterojunction are calculated as follows [30]:

$$\alpha(\omega) = (\sqrt{2})\omega[\sqrt{\varepsilon_1(\omega)^2 + \varepsilon_2(\omega)^2} - \varepsilon_1(\omega)]^{1/2}. \quad (2)$$

Where α refers to absorption coefficients as the function of optical frequency ω.

3. Results and discussion

3.1. Geometric configuration

In recent years, the synthesized 2D perovskite with the formula $A_{n+1}M_nX_{3n+1}$ (A = Cs, M = Pb, Sn, and X = Cl, Br, I) attracted much attention due to the stability compared with 3D hybrid perovskite [16]. Taking into consider the limitation of computing sources, we employ 2D single-layer inorganic Cs_2PbI_4 ($n = 1$) perovskite and black phosphorus to construct heterojunction to investigate their physical properties for simplicity. The unit cell of Cs_2PbI_4 perovskite belongs to orthorhombic system with pnma space group (shown in figure 1(a)), and the optimized lattice parameters are $a = 6.37$ Å, $b = 6.37$ Å, $c = 19.48$ Å, respectively. The unit cell of black phosphorus crystalline is in orthorhombic system with space group cmca [15], and the lattice constants are $a = 4.56$ Å, $b = 3.31$ Å, $c = 11.32$ Å, respectively [31]. (shown in figure 1(b)). We select crystal plane (0 0 1) of Cs_2PbI_4 and black phosphorus to construct semiconductor heterostructures as layered octahedral PbI_6 and black phosphorus are separated along (0 0 1) axis, hence cleaving surface along crystal plane (0 0 1) can effectively reduce dangling bonds. Figures 1(c) and (d) illustrate the optimized atomic structures of 2D Cs_2PbI_4-black phosphorus heterojunction with Cs–I and Pb–I interfacial contacts, respectively. Two kinds of terminate contacts are designed to investigate the influence of interfacial engineering on photovoltaic performance. A 15 Å vacuum region were added to minimize the interactions between the neighboring atoms, and the lattice mismatch was less than 2.3%. The calculated minimum distance between the crystal plane (0 0 1) of 2D perovskite Cs_2PbI_4 and the black phosphorus with Cs–I and Pb–I terminates are 3.32 Å and 3.35 Å, respectively, indicating the Cs_2PbI_4–P structure is van der Waals heterojunction. Formation energies of Cs_2PbI_4–P heterojunction for two kinds of configurations were calculated to evaluate their thermal stability and interfacial interaction according to the following equation: $E_b = E_{heter} - E_{Cs_2PbI_4} - E_P$, where E_{heter}, $E_{Cs_2PbI_4}$ and E_P indicate the total energies of 2D heterojunction, layered perovskite Cs_2PbI_4 and black phosphorene, respectively. Table 1 lists formation energies of both interfacial contacts are -1.37 eV and -1.507 eV for Cs–I, Pb–I terminal, respectively. Both interface formation are exothermic due to negative formation energies, revealing two kind of heterojunction can be formed. Therein, the calculated data reveal Pb–I interface is more stable than Cs–I interface owing to lower formation energy.

3.2. Electronic structure

The band structures of 2D perovskite, black phosphorene and heterojunction were calculated by using HSE06 functional method as standard GGA–PBE method usually underestimate band gap. Figures 2(a) and (d) illustrate the band structure

(a) (b) (c)

Cs-I interface

(d) (e) (f)
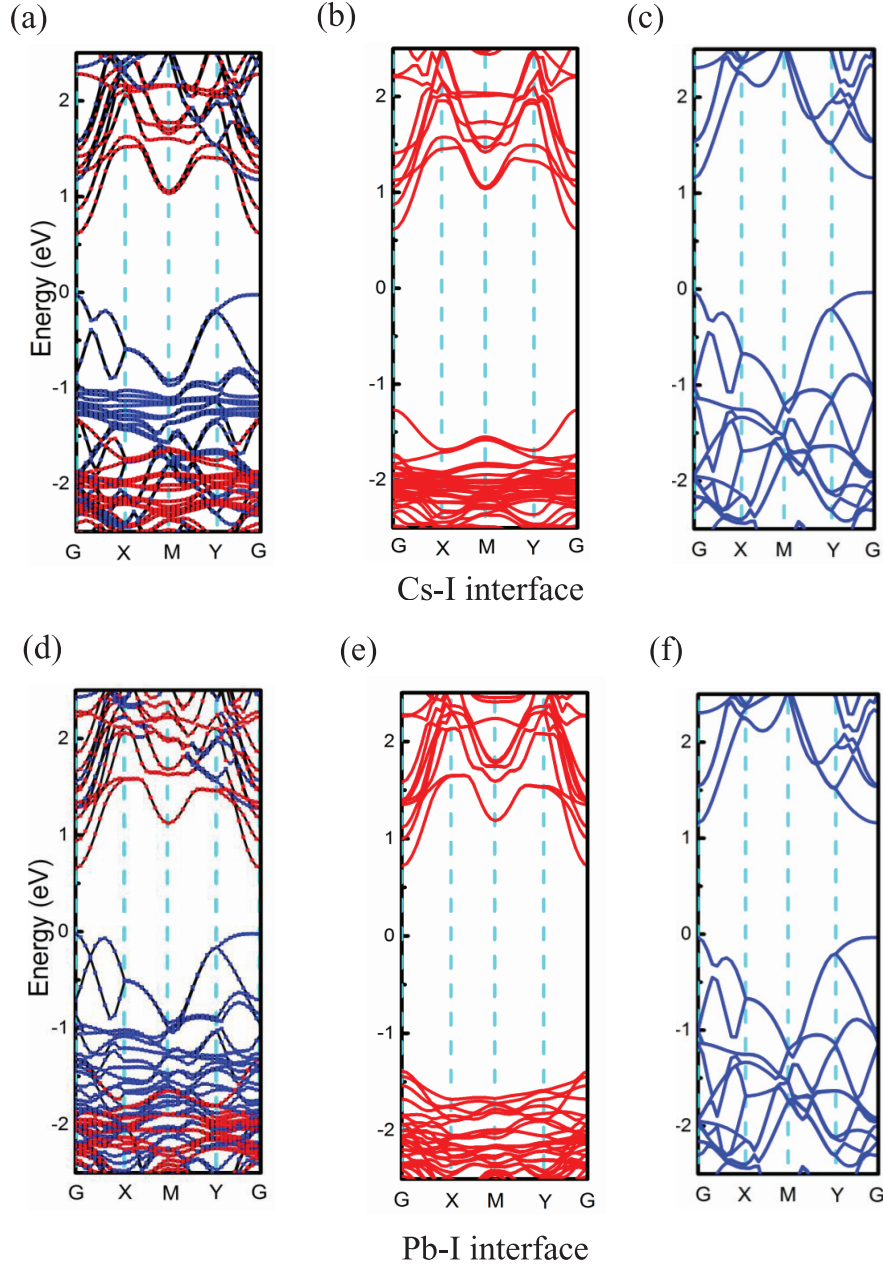
Pb-I interface

Figure 2. Decomposed electronic band structures of (a) Cs–I interface semiconductor heterojunction, (b) Cs–I interface, (c) black phosphorous, (d) Pb–I interface semiconductor heterojunction, (e) Pb–I interface, (f) black phosphorous. The red and blue lines represent the electronic orbital contributions of Cs_2PbI_4 and black phosphorous, respectively. The fermi level is set at zero. The high-symmetry points in the first Brillouin zone (FBZ) are $G(0\,0\,0)$, $X(0.5\,0\,0)$, $M(0.5\,0.5\,0)$, $Y(0\,0.5\,0)$, respectively.

of heterojunction Cs_2PbI_4–P along with projected atomic orbital energy of partial Cs_2PbI_4 and P indicated by red and blue colour, respectively. Figures 2(b), (c), (e) and (f) demonstrate band structure of free-standing 2D structure Cs_2PbI_4 and P. The calculated results reveal total band structure of heterojunction can be considered as a direct superposition of free-standing Cs_2PbI_4 and P for both interfacial contacts. Thus, interfacial interaction between Cs_2PbI_4 and P presents weak Van der Waals force, and the results are in agreement with calculated geometric configuration, which exhibits large distance between interfaces. As illustrated in figures 2(a) and (d), both interfacial contacts are type II band alignments

Table 2. Calculated electron–hole effective masses of 2D Cs_2PbI_4–P heterostructure with Cs–I and Pb–I interfacial contacts along $G \rightarrow X$ and $G \rightarrow Y$ direction, respectively.

	Cs–I interface		Pb–I interface	
	m_e^*	m_h^*	m_e^*	m_h^*
$G{\rightarrow}X$	3.48	0.32	3.93	0.35
$G{\rightarrow}Y$	0.39	0.43	0.37	0.41

where conduction band minimum (CBM) and valence band maximum (VBM) are mainly occupied by electronic orbital levels of Cs_2PbI_4 and P, respectively. Differing from indirect
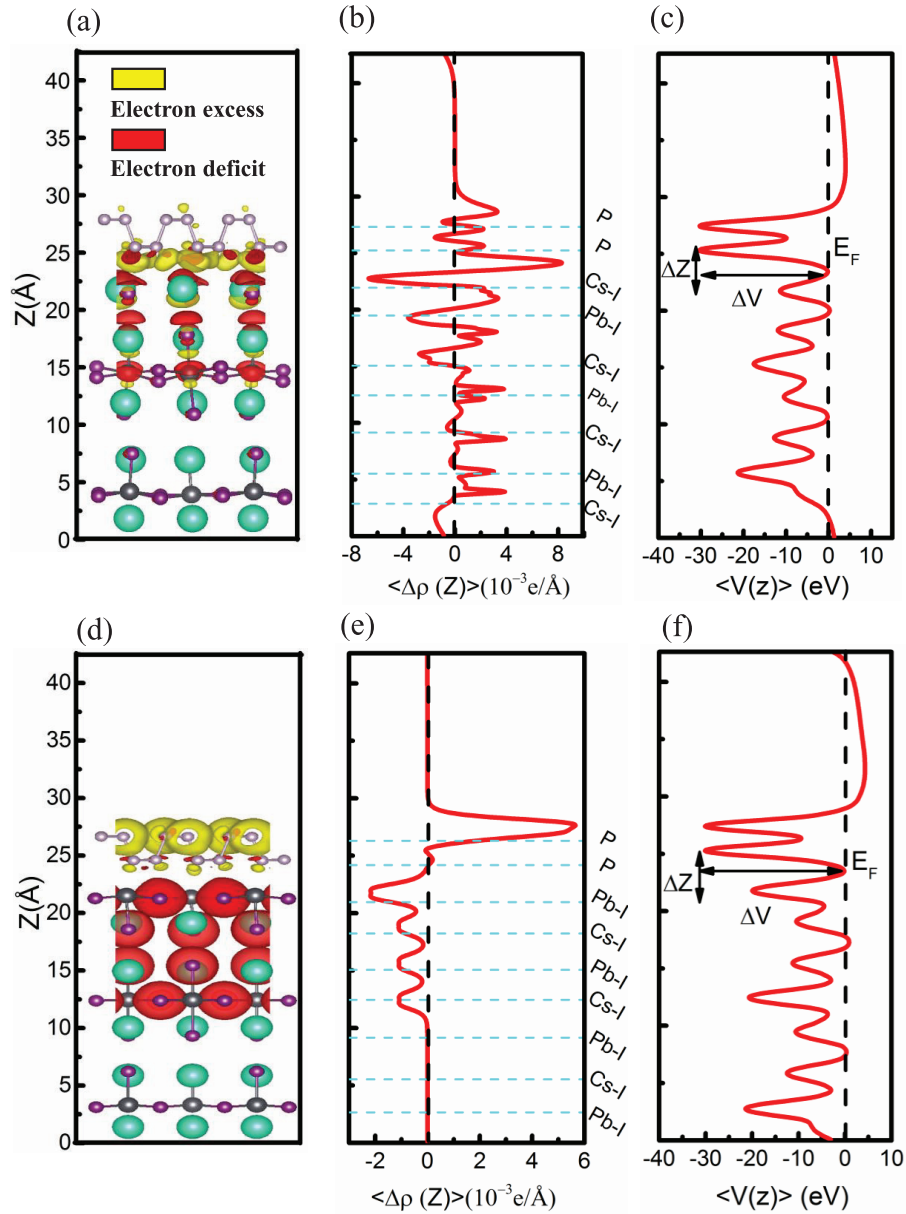
Figure 3. (a) and (d) The charge density difference, (b) and (e) planar-averaged differential charge density $\Delta\rho(z)$, (c) and (f) plane-averaged electrostatic potential $\Delta V(z)$ along Z direction of Cs–I and Pb–I interfacial heterojunction.

band gap of 3D CsPbI$_3$–P heterojunction reported by Liu [32], 2D Cs$_2$PbI$_4$–P heterojunction exhibits direct band gap at high symmetric G point, which being more favorable for photogenerated electron transition than 3D CsPbI$_3$–P without phonon assistance. This direct band gap, of course, contributes greatly to the improvement of photovoltaic performance. The calculated band gaps of 2D heterojunction for Cs–I and Pb–I interface contacts are 0.64 eV and 0.68 eV, respectively, which are below the values of free-standing Cs$_2$PbI$_4$ and phosphorus. By fitting the second order parabola according to equation (1), electron–hole effective masses along $G \to X$ and $G \to Y$ direction were calculated, listed in table 2. The results reveal charge carrier effective masses for both interfaces along $G \to Y$ direction are basically similar and present small order of magnitude, being conducive to charge carrier

transport. However, hole effective masses for two interfacial contacts are much larger than those of electron along $G \to X$ direction, which hinder the high carrier mobility.

In order to further understand how to generate charge carrier by light Illumination, The total density of states (TDOS) and the partial density of states (PDOS) of Cs$_2$PbI$_4$–P heterostructure with Cs–I, Pb–I interfacial contacts were calculated by using HSE06 functional method, as shown in figures 1S(a) and (b) (see supporting information (stacks.iop. org/JPhysCM/32/195501/mmedia)). The results demonstrate photogenerated charge carriers are mainly contributed from the electron transition of P-p orbitals in valence band maximum to Pb-p orbitals in conduction band minimum, being different from the I-p orbital transition to Pb-p orbitals in classical 3D perovskite MAPbI$_3$ [33–35].
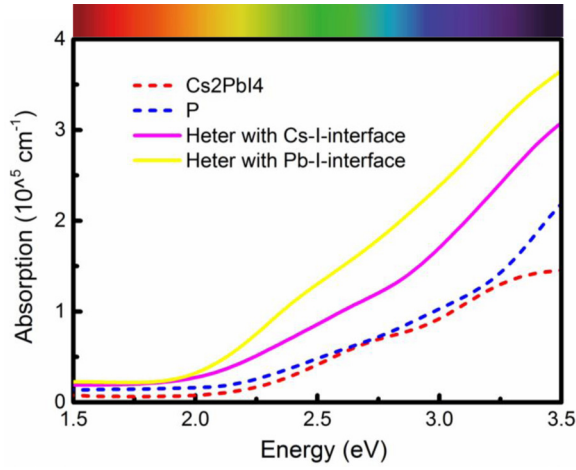
Figure 4. Optical absorption coefficients of perovskite Cs_2PbI_4, phosphorene and heterostructure Cs_2PbI_4–P with Cs–I and Pb–I interfacial contacts, respectively.

3.3. Charge transferring

Nonradiative recombination rates of electron–hole pairs at the interface is an important factor to restrict the photoelectric conversion efficiency of solar cells. Here we qualitatively and quantitatively investigated the charge transferring of 2D Cs_2PbI_4–P heterojunction by considering two interfacial contacts i.e. Cs–I, Pb–I interface as comparison. The plane-averaged charge density difference $\Delta\rho(z)$ can be expressed as $\Delta\rho(z) = \rho_{heter} - \rho_{Cs_2PbI_4} - \rho_P$, where ρ_{heter}, $\rho_{Cs_2PbI_4}$ and ρ_P represent the plane-averaged charge density of the heterostructure, free-standing Cs_2PbI_4 and phosphorene, respectively. Analysis of the charge density difference of the Cs_2PbI_4–P heterojunction with different Cs–I, Pb–I interfacial contacts reveal the same interesting charge-redistribution phenomenon, in which the inhomogeneous Cs_2PbI_4 and phosphorene induce hole- and electron-rich regions, respectively (figures 3(a) and (d)). As seen in figures 3(a) and (d), interfaces of phosphorene accumulate electrons indicated by yellow region while electrons in interface of Cs_2PbI_4 dissipate indicated by red region. To further clarify the charge redistribution, the plane-averaged charge density difference $\Delta\rho(z)$ was extracted parallel to the planes of Cs_2PbI_4 and phosphorene (figures 3(b) and (e)). There exhibits an obvious charge transfer from interface of Cs_2PbI_4 to that of phosphorene across the junction. Furtherly, a detail bader charge analysis is employed for quantitative assessment of charge transferring for each type of element. As shown in figures S2(a) and (b), total 0.385|*e*| migrate from Cs–I to phosphorene while 0.324|*e*| transfer from Pb–I interface to phosphorene. The calculated results reveal Cs–I interface is more conducive to charge transfer at the interface and reduce the recombination rates of electron–hole pairs. It is also intriguing that Cs element plays important role in the interfacial charge transport to provide about 8.239|*e*| and 8.376|*e*| for Cs–I and Pb–I interface in spite of that orbital electrons of Cs element are far from band edge, thus contribute little to the photogenerated carriers. Figures 3(c) and (f) show the plane-averaged electrostatic potential $\Delta V(z)$ along the perpendicular direction of the 2D Cs_2PbI_4–P heterojunction. The averaged

electrostatic potential $\Delta V(z)$ drop from perovskite layer to phosphorene across heterojunction and the drop values are found to be about 17 eV and 10 eV for Cs–I and Pb–I interface, respectively. Such a large potential difference implies a strong built-in electrostatic field across the interface, which may be the origin of electron migration and significantly influence the charge injection and carrier dynamics.

3.4. Optical property

According to the equation (2) listed in method section, optical absorption coefficients of free-standing Cs_2PbI_4, P and 2D Cs_2PbI_4-P heterostructure were calculated, as shown in figure 4. The optical absorption coefficients of P is a little larger than those of Cs_2PbI_4 in the visible light region. While considering the combined heterojunction, the optical absorption coefficients of both interfacial contacts. i.e. Cs–I and Pb–I terminal, indicated by yellow and purple colour, are significantly greater than those of two completely freestanding structure Cs_2PbI_4 and P. These results demonstrate 2D Cs_2PbI_4–P heterostructure belongs to type II heterojunction with narrower optical gap, which being in well agreement with above calculated electronic structures. Moreover, the calculated optical absorption coefficients of Pb–I interfacial contact are larger than those of Cs–I interface, indicating more superior light harvesting ability.

4. Conclusion

In summary, the geometric construction, electronic structure, charge carrier property and optical absorption coefficients of 2D heterostructure Cs_2PbI_4–P were investigated based on first-principles calculations. The 2D heterostructure Cs_2PbI_4–P can be formed due to negative formation energy, and the large distance above 3 Å as well as direct superposed band structure between Cs_2PbI_4 and P layer indicates the heterojunction belongs to be Van der Waals heterojunction with weak interaction. The Cs_2PbI_4–P heterostructure possess favorable type II band alignment with narrower direct band gap comparing with free-standing Cs_2PbI_4 and P. Under visible-light irradiation, photogenerated electrons jump from the valence band occupied by P-*p* orbital to conduction band of Pb-*p* orbital. With regard to comparison of Cs–I and Pb–I interface, The heterostructure for both cases exhibit smaller effective masses along $G \rightarrow Y$ direction. In addition, Cs–I interface exhibits more strong charge transferring from Cs_2PbI_4 to P than that of Pb–I interface due to the larger potential difference between the Cs_2PbI_4 and P layers. Furthermore, the optical absorption coefficients of constructed Cs_2PbI_4–P heterostructure with two interfacial contacts are larger than those of free standing Cs_2PbI_4 and P attributed to type II heterojunction, in which Pb–I interface demonstrates higher optical absorption property. Our results exhibit the photovoltaic property of 2D Cs_2PbI_4–P heterostructure from an atomic level and provided a theoretical guidance for the electrical interfacial engineering to design high efficient 2D perovskite based heterostructures.

Acknowledgments

ORCID iDs

Yu-Qing Zhao ⓘ https://orcid.org/0000-0001-8073-5346
Dai-Feng Zou ⓘ https://orcid.org/0000-0002-5645-180X
Meng-Qiu Cai ⓘ https://orcid.org/0000-0002-5364-725X

References

[1] Filip M R, Eperon G E, Snaith H J and Giustino F 2014 *Nat. Commun.* **131** 5757
[2] Noh J H, Sang H I, Jin H H, Mandal T N and Sang I S 2013 *Nano Lett.* **13** 1764–9
[3] Stranks S, Eperon G, Grancini C, Menelaou C, Alcocer M, Leijtens T, Herz L, Petrozza A and Snaith N 2013 *Science* **342** 341–4
[4] Xing G, Mathews N, Sun S, Lim S, Lam Y M and Grätzel M 2013 *Science* **342** 344–7
[5] Kim M *et al* 2019 *Joule* **3** 2179–92
[6] Pazos-Outon L M *et al* 2016 *Science* **35** 1430–3
[7] Jodlowski A D, Roldán-Carmona C, Grancini G, Salado M, Ralaiarisoa M, Ahmad S, Koch N, Camacho L, de Miguel G and Nazeeruddin M K 2017 *Nat. Energy* **2** 972–9
[8] Zhao X G, Yang J H, Fu Y, Yang D W, Xu Q L, Yu L P, Wei S H and Zhang L J 2017 *J. Am. Chem. Soc.* **139** 2630–8
[9] Zhao Y Q, Ma Q R, Liu B, Yu Z L and Cai M Q 2018 *Phys. Chem. Chem. Phys.* **20** 14718–24
[10] Zhu X L, Liu P F, Zhang J R, Zhang P, Zhou W X, Xie G F and Wang B T 2019 *Nanoscale* **11** 119923–32
[11] Xie G F, Ju Z F, Zhou K K, Wei X L, Guo Z X, Cai Y Q and Zhang G 2018 *NPJ Comput. Mater.* **4** 21
[12] Christians J A, Miranda Herrera P A and Kamat P V 2015 *J. Am. Chem. Soc.* **137** 1530–8
[13] Dou L *et al* 2015 *Science* **349** 1518–21
[14] Dong J Y, Ma Z Q, Yang Y, Wang S P and Pan H 2019 *Molecules* **24** 2144–55
[15] Ding Y F, Zhao Q Q, Yu Z L, Zhao Y Q, Liu B, He P B, Zhou H, Li K L, Yin S F and Cai M Q 2019 *J. Mater. Chem.* C **7** 7433–71
[16] Bala A, Deb A K and Kumar V 2018 *J. Phys. Chem.* **122** 7464–73
[17] Dai J and Zeng X C 2014 *J. Phys. Chem. Lett.* **5** 1289–93
[18] Yang J, Xu R J, Pei J J, Myint Y M, Wang F, Wang Z, Zhang S, Yu Z F and Lu Y R 2015 *Light Sci. Appl.* **4** e312
[19] Cai Y, Zhang G and Zhang Y W 2014 *Sci. Rep.* **4** 6667
[20] Liu B, Long M Q, Cai M Q and Yang J L 2018 *J. Phys. Chem. Lett.* **9** 4822–7
[21] Zhang L, Lin S, Wu B, Li Q F and Li J F 2019 *J. Mol. Graph. Model.* **89** 96–101
[22] Chen K Q, Wang Y W, Liu J F, Kang J L, Ge Y Q, Huang W C, Lin Z T, Guo Z N, Zhang Y P and Zhang H 2019 *Nanoscale* **11** 16852–9
[23] Yang D J, Du Y H, Zhao Y Q, Yu Z L and Cai M Q 2019 *Phys. Status Solidi* b **256** 18005401–6
[24] Kresse G and Furthmüller J 1996 *Phys. Rev.* B **54** 11169–86
[25] Kresse G and Furthmüller J 1996 *Comput. Materi. Sci.* **6** 15–50
[26] Blöchl P E 1994 *Phys. Rev.* B **50** 17953–79
[27] Perdew J P, Burke K and Ernzerhof M 1996 *Phys. Rev. Lett.* **77** 3865–8
[28] Dion M, Rydberg H, Schroder E, Langreth D C and Lundqvist B I 2004 *Phys. Rev. Lett.* **92** 246401
[29] Heyd J, Scuseria G E and Ernzerhof M 2003 *J. Chem. Phys.* **118** 8207–15
[30] Gajdos M, Hummer K, Kresse G, Furthmuller J and Bechstedt F 2006 *Phys. Rev.* B **73** 0451121–9
[31] Qiao J S, Kong X H, Hu Z X, Yang F and Ji W 2014 *Nat. Commun.* **5** 4475
[32] Liu B, Long M Q, Cai M Q and Yang J 2018 *Appl. Phys. Lett.* **112** 043901
[33] Liao C S, Zhao Q Q, Zhao Y Q, Yu Z L, Zhou H, He P B, Yang J L and Cai M Q 2019 *J. Phys. Chem. Solid.* **135** 109060
[34] Yu Z L, Zhao Y Q, He P B, Liu B, Yang J L and Cai M Q 2020 *J. Phys.:Condens. Matter* **32** 065002
[35] Deng X Z, Zhang J R, Zhao Y Q, Yu Z L, Yang J L and Cai M Q 2020 *J. Phys.:Condens. Matter* **32** 065004